Pergamon

PII: S0191-8141(96)00012-0

Journal of Structural Geology, Vol. 18, No. 8, pp. 1061 to 1077, 1996

0191-8141/96 $15.00+0.00

Development of strike-slip faults: shear experiments in granular materials and clay using a new technique

L.-J. AN* and C. G. SAMMIS

Department of Earth Sciences, University of Southern California, University Park, Los Angeles, CA 90089-0740, U.S.A.

(*Received* 24 *June* 1994; *accepted in revised form* 26 *January* 1996)

Abstract—A new experimental technique has been developed to study fault development in layers of moist granular materials (clay and fault gouge) in shear. Faults nucleated on pre-existing pores and on low-displacement protofaults in flaw-free areas. Only a small number of the protofaults developed significant displacement, forming conjugate simple fault sets. After nucleation, simple faults propagated in-plane. As these simple faults grew in length and new simple fault sets nucleated, they began to interact and coalesce. Simple faults linked up to form compound faults, and compound faults linked up to form even larger through-going strike-slip faults. The fault patterns produced in the shear experiments were integrated fault networks consisting of several sets of conjugate shears and tensile structures. Compound faults exhibited both releasing and restraining steps formed during fault coalescence. Displacement along such a compound strike-slip fault caused a mismatch of the two walls. A few points became resistant barriers while the remaining segments became pull-apart basins. Both releasing and restraining steps led to the development of pull-apart basins. Fault displacement and propagation rate were linear functions of fault length. The difference between the experiment described here and traditional Riedel experiments is that the new experiments do not have a pre-existing fault in the experimental setup. Therefore they are more suitable to study fault nucleation and evolution in a broad shear zone. Copyright © 1996 Elsevier Science Ltd

INTRODUCTION

A fundamental problem in structural geology and rock mechanics is understanding the nucleation, growth and interaction of faults which form fault networks in a broad zone under simple shear stress. This understanding can give us knowledge about the tectonic evolution of the crust (Sylvester 1988), earthquake mechanisms (Wesnousky 1989), basin development (Crowell 1974), underground fluid flow systems (Wang 1991), and the engineering properties of rock mass (Jaeger & Cook 1976).

Previous field studies have indicated that strike-slip faults may nucleate on joints (Segall & Pollard 1983, Martel 1990). In the laboratory, shear cracks have been observed to nucleate from tensile crack arrays (Peng & Johnson 1972, Cox & Scholz 1988, Reches & Lockner 1994). Once nucleated, the growth mechanism of strike-slip faults has been more problematic. Field geologic studies measure hundreds of kilometers of shear displacement along large strike-slip faults. It might seem obvious that these strike-slip faults have extended as in-plane shears. However most laboratory experiments fail to produce in-plane shear propagation (Brace & Bombalakis 1963, Lajtai 1971, Horii & Nemat-Nasser 1985, Sammis & Ashby 1986). Petit & Barquins (1988) and Reches & Lockner (1994) have observed in-plane propagation of shear cracks, but the shear cracks did not grow simply as mode II (in-plane shear) but as damaged zones caused by collapse of tensile fault arrays. Mode II has therefore been ruled out as a basic mode of propagation by Petit & Barquins (1988).

Fault interaction is a less explored area. Field geologic investigations have found steps, pull-apart basins, and upwarps along strike-slip faults which indicate fault interaction (Crowell 1974, Sibson 1985, Deng *et al.* 1986, Wesnousky 1989). Theoretical studies of fault interaction generally assume two parallel pre-existing faults in a homogeneous medium, and solve for the stress field in the interacting region by using either the principle of superposition (Chen 1984, Horii & Nemat-Nasser 1985, Kachanov 1987), the method of successive approximation (also called Schwarz alternating technique, see e.g. Segall & Pollard 1980, Aydin & Schultz 1990) or an asymptotic approximation (Chang 1982, Du & Aydin 1991). Theoretical studies (Du & Aydin 1993) and laboratory experiments (Lin & Logan 1991, Shen *et al.* 1995) of fault propagation path indicate that two non-coplanar faults first overlap and then link up forming a longer fault. Two strike-slip faults can link in either a right- or left-step arrangement in the same shear field (Du & Aydin 1993). These studies are all limited in that they do not consider the interaction of more than two faults, or the conjugate geometry of shear structures.

One of the most important techniques commonly used to study the development of strike-slip faults is clay cake experiments performed under directly applied shear strain. These experiments can be classified into two categories: Riedel shear and distributed shear. In the Riedel experiment a slab of clay is placed horizontally on two parallel adjacent boards. As one board is slid horizontally past the other, a network of faults develops

*Now at Tidelands Oil Production Company, Long Beach, CA 90801-1330, U.S.A.

in the overlying clay layer (Cloos 1928, Riedel 1929, Tchalenko 1970, Wilcox *et al.* 1973, Naylor *et al.* 1986, Withjack & Jamison 1986, Smith & Durney 1992). Because the sliding boundary between the two boards is a boundary condition, all structures generated during the experiment are secondary ones with respect to the pre-existing 'fault' and therefore they are not suitable for studying the origin of crustal shear zones.

Several different apparatus have been designed to study the development of fault patterns under distributed shear strain. Hoeppener *et al.* (1969) and Gapais *et al.* (1991) deformed their clay and sand samples using deformation boxes. They generated fault patterns dominated by antithetic faults. Freund (1974) and Schreurs (1992, 1994) used an apparatus with a layer consisting of thin bars stacked as cards between the moving boards and the sample layer. They generated fault patterns dominated by synthetic faults. Because these experiments maintained a constant sample width perpendicular to the shear direction, they produce true 2-D simple shear. Simple shear simulates fault development at small strain when displacements along faults are not significant. At large strain an additional tensile stress is needed to maintain a simple shear strain (constant sample width) since a sample has to be stretched, and the magnitude of this tensile stress increases with shear strain. In the crust, however, such a tensile stress may not exist. Instead there is a compressional stress component due to confining pressure. To simulate natural strike-slip faulting at large strain, either the applied shear stress should rotate with progressive shear deformation, or a confining pressure must be applied. An alternative way to solve the problem is to allow lateral contraction of a sample associated with shear strain. An experiment of this type was performed by Cloos (1955). A piece of square wire cloth was used at the base of the clay cake. Shear deformation was achieved by fixing one side of the wire cloth while moving the opposite side laterally. Sample width decreased during these experiments. Distributed conjugate strike-slip faults were developed, and macroscopic rotation and lateral shortening (perpendicular to applied shear direction) were also observed.

In this paper, we introduce a new experimental technique to achieve a shear deformation over a broad zone which can be used to model the strike-slip faulting process up to relatively large strain. Each experiment begins as simple shear deformation but as shear strain becomes large, the sample is free to shorten laterally (perpendicular to the applied shear stress) under cohesive force of the material. The deformation at large strain is thus no longer simple shear, but contains a component of lateral shortening. We again emphasize that our experiment differs from Riedel shear experiment in that it does not use any pre-existing fault as a boundary condition. It differs from the wire cloth experiments in that the base of our layer is less constrained. For the fault networks produced, we observed and quantified: (1) fault nucleation, (2) fault propagation, (3) fault interaction and coalescence, (4) fault patterns, (5) fault barriers and pull-apart basins, (6) the scaling relationship between fault length and shear displacement and (7) the scaling relationship between fault length and its growth rate.

EXPERIMENTAL METHOD

We used gravity sliding to achieve shear deformation of moist granular and clay layers. Fine-grained fault gouge and clay were chosen because these materials are less elastic than rocks, which allows observation of the dynamic evolution, and because the strain field associated with faulting in clay has been observed to be similar to that predicted by elastic dislocation calculations (Hildebrand-Mittelfeldt 1979). Experimental results from clay layers have been shown to be applicable directly to rock by Bartlett *et al.* (1981). Some field observations indicate that the Earth's crust has a granular structure (Gallagher 1981, Scott *et al.* 1993) which raises the possibility that our experimental results might be directly applicable to large scale geological structures. The sample dimension was 80 × 40 × 2.3 cm which proved large enough for the propagation and interaction of a multitude of faults ultimately leading to through-going shear zones. The sample was totally exposed so that the faulting process from nucleation to interaction was visible and camera-recordable.

The apparatus used to perform the shear experiment is shown in Fig. 1(a). An aluminum board (60 × 120 cm) with raised edges was fitted with an axle so that it could be tilted at any angle up to 90°. A rope and pulley system was used to adjust and maintain the tilt angle.

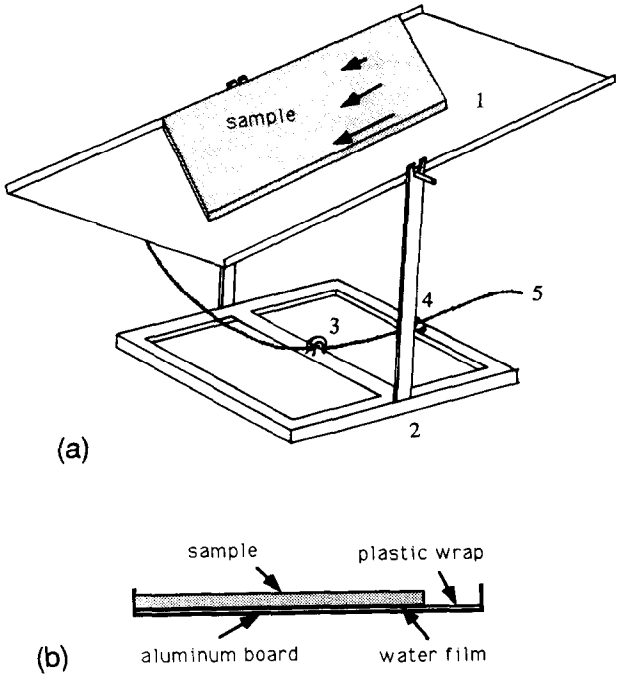

Fig. 1. (a) is the apparatus used for the simple shear experiment. 1. aluminum board, 2. holder, 3. pulley, 4. pulley lock, 5. rope. Arrows show displacement in a sample. (b) is a cross section of a loaded sample.

Sample preparation

Fault gouge from San Andreas and San Gabriel faults and clay were used to make the experimental layers. Natural gouge was used because our experiments showed that moist gouge is less cohesive than clay, and therefore is suitable for simulating brittle deformation. Natural gouge has a power-law distribution of grain sizes from 2 μm to more than 1000 μm (Sammis *et al.* 1987, An & Sammis 1994) but in this study we only used the fine fractions with a grain size smaller than 125 μm. The fractal structure of gouge in which smaller grains fill-in the space formed by larger grains at all scales produces very small pore-sizes, and may mimic the multiscale heterogeneity thought to characterize the crust. Water content in the moist samples was controlled and estimated by comparing the weight of wet and dry samples. A suitable water content was determined by repeated testing. For both gouge and clay, about 39% water by weight allowed these materials to transmit stress during deformation, and yet remain soft enough to deform under gravity loading. A sample was loaded as shown in Fig. 1(b). The board was set in the horizontal position, moistened with water and then covered with a layer of plastic kitchen wrap. The plastic layer reduced friction between the board and the clay or gouge layer. A thin film of water was spread on top of the plastic wrap to further reduce the friction. Only the surface of the board, not the raised edge, was covered with plastic, so that the sample could slide down the plastic-covered surface upon tilting while remaining fixed to the uncovered edge, thereby generating the shear strain. A rectangular frame (80 × 40 cm) was placed on top of the board, with the raised edge of the board as one side and three plastic rails for the other sides. The moist granular material was loaded into the frame to produce a flat layer of uniform thickness of 2.3 cm. The frame was removed after two hours. A square grid was inscribed on the sample surface to monitor strain. In some experiments we tried corn oil as a lubricant, but it was found that for this lower boundary condition, strain became localized near the attached edge leading to a tearing of the sample near the edge.

Experimental procedure

An experiment was started by tilting the board (Fig. 1a). The sample layer usually began to move at a tilt angle of about 30°. Deformation took place first near the fixed edge, then spread toward the opposite free edge due to strain hardening. A uniform shear deformation was achieved once the shear deformation swept the whole region and it remained uniform thereafter. For a few experiments, the board was also tilted laterally to apply a 'confining pressure'.

In order to understand the mechanics of layer movement, let us assume that a sample can be divided into numerous rectangular zones (Fig. 2a). Because sample thickness is uniform, the gravity force within each zone is the same, i.e. F1 = F2 = F3 = ... = Fn. If no boundary of the sample is fixed, all the zones will move at the same speed. However if one boundary is fixed as in the experiment, then the zone closest to the fixed edge (zone 1) experiences greater than average shear strain at the beginning. It then dilates and hardens, and strain moves to the zone 2 of lower strain. The zone 2 can then transfer strain to zone 3 after it hardens, and so forth until shear strain becomes uniform (Fig. 2b).

The hardening may be caused by two mechanisms. One is strain hardening related to shear deformation within the sample. The other is basal frictional hardening. When corn oil is used as basal lubricant, strain hardening does not occur, and the sample fails along a narrow localized shear zone near the fixed edge. This implies that hardening with water as a lubricant occurs mostly at the base, probably as a result of water absorbed in the dilating material. Basal friction plays at least three important roles: resisting rotation accompanying shear, resisting sliding, and inducing shear strain by resisting further deformation in the more strained zones. Basal friction force F_Θ can be expressed as:

$$F_f = -[\mu(F_n + A\Delta P) + AS_0] \quad (1)$$

where μ is the coefficient of basal friction, F_n is normal force, ΔP is the difference between confining pressure P and pore pressure P_p ($\Delta P = P - P_p$), A is the area of the zone, and S_0 is the inherent shear strength of the surface. As shown in Fig. 2(a) when one zone is more strained

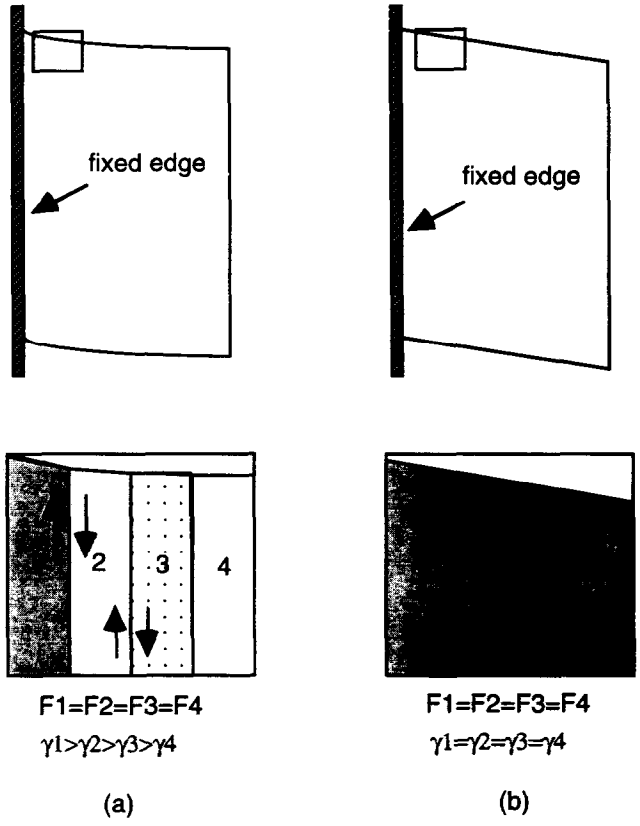

Fig. 2. Sketch showing how deformation evolves from initial non-uniform in (a) to finally uniform simple shear in (b). Deformation in each small box in (a) and (b) is enlarged in the lower parts. Fn and γn denote gravity force and shear stress in nth zone. Shadows show the extent of strain.

(shaded darker) than another, the dilation of the zone causes pore pressure to drop within that zone (ΔP to increase in Eqn 1). The lower pore pressure has two impacts. One is to cause water to be sucked up from the sample-board interface into pores. The loss of lubricant between the interface increases basal friction. Because corn oil is a nonwettable phase, it cannot be absorbed by the pores and thus it does not cause frictional hardening. The pore pressure drop is equivalent to an increase in normal stress which also produces an increase in basal friction according to Eqn (1). The effect is to resist the movement of the more strained minizone and transfer strain to the less strained minizones.

The subsequent deformation is maintained uniform by the same mechanism. Because of hardening due to increase in basal friction, the sample had to be continually tilted in order to maintain a constant deformation rate.

We used scaling arguments to choose an experimental strain rate of 10^{-4} s^{-1}. There is evidence that the Earth's crust is in a critical state in the sense that strain rates occur to maintain stress levels near the shear strength σ^* (Turcotte, 1991). If we assume viscous deformation, then deformation rate $\dot{\varepsilon}$ is

$$\dot{\varepsilon} = \frac{\sigma^*}{\eta} \tag{2}$$

where η is viscosity. For the crust, η is appropriately 10^{21} Pa.s (Yang & Toksoz 1981, Ito 1983) and σ^* is on the order of 10^8 Pa (Jaeger & Cook 1976). So $\dot{\varepsilon}$ should be about 10^{-12} s^{-1}, in agreement with independent estimates (Pfiffner & Ramsay 1982, An & He 1987, Carter & Tsenn 1987). For clay with water content similar to those used in our experiments, σ^* is about 10^3 Pa (Mitchell 1993) and η is about 10^7 Pa.s (Ramberg 1981), so $\dot{\varepsilon}$ should be about 10^{-4} s^{-1} if the clay is to flow at a stress near σ^* as postulated. During the experiments, strain rate was monitored by measuring the displacement velocity on the vertical free edge. The strain rate of a sample slowed to a stop if the tilt angle was maintained constant, presumably due to the strain hardening or basal friction increase caused by internal pressure drop within the samples, as discussed above. In order to maintain a constant strain rate at 10^{-4} s^{-1}, the inclination of the apparatus was continually increased throughout the experiment.

Two methods were used to calculate shear strain λ. One was by measuring the original length l of a square marker and the shear displacement d after deformation, and strain was calculated as d/l. The other method was to calculate strain from the width w and shear displacement $\bar{d}$, of an entire sample layer. The strain was $\bar{d}/w$.

The nucleation and evolution of the shear structures within a sample layer were followed visually and photographically. Low-angle lighting was used from different directions to enhance structures of various orientations. More detailed analyses were performed later by studying these pictures. To minimize boundary effects, only those structures developed at least 10 cm from a boundary were analyzed. An experiment was stopped when the layer lost coherence, or when the tilt angle approached 90°. Each experiment lasted for about 4 hours.

EXPERIMENTAL OBSERVATIONS

Figures 3 and 4 show the development of structures in gouge and clay layers during the shear experiments. Faulting sequences in the two types of materials are summarized in Table 1. In general, a fault started as a myriad of protofaults, a few of which grew into simple faults. Several simple faults then interacted and coalesced to form a compound fault (Figs. 3 and 4). In this paper we use the term 'protofault' to refer to a type of low-displacement linear trace observed on a sample surface at a very early stage of the deformation. The term 'simple fault' refers to a fault developed simply by in-plane extension, and 'compound fault' refers to a fault formed by coalescence of simple faults (see Martel 1990). For convenience a simple strike-slip fault is also called a shear.

Protofault stage

At the onset of loading, a sample first experienced dilation as evidenced by open pores and the disappearance of water from the sample surface due to absorption into the open pores. Fault development then began with the development of low-displacement protofaults in defect-free areas (see Figs. 3a and 4a). The protofaults exhibited no measurable offset, but they were approximately ten centimeters long when they became visible. The protofaults were conjugate: one set trended 21 ± 2° in gouge (13 ± 2° in clay layer) and the other set trended 79 ± 2° (82 ± 4° in clay layer) clockwise from applied shear direction (Table 1). The applied shear direction is right-lateral, as shown by the half arrows, in Figs. 3 and 4. The protofaults were faint but very dense: the spacing between the protofaults was only about 0.5 mm.

In the areas where defects (mostly visible pores) existed, faults nucleated directly from the defects and began to propagate in conjugate shear directions. Only a relatively small number of faults nucleated in this way.

Simple fault stage

As deformation continued, shear displacement along some of the protofaults became detectable and, by our definition, these protofaults became simple faults. We call the two conjugate simple fault sets primary shears. The synthetic set is denoted by symbol S_1 and the antithetic set, by S_1'. Only a small portion of protofaults became simple faults. The remaining protofaults between simple faults were abandoned (Figs. 3b and 4b) as all the shear deformation was accommodated by displacement on the simple faults. The intervals between the simple faults were approximately equal: about 12 mm in the gouge layer and 7 mm in the clay layer.

Once nucleated, simple faults propagated in their own planes (Figs. 3b–d and 4b–d). The S_1 shears propagated

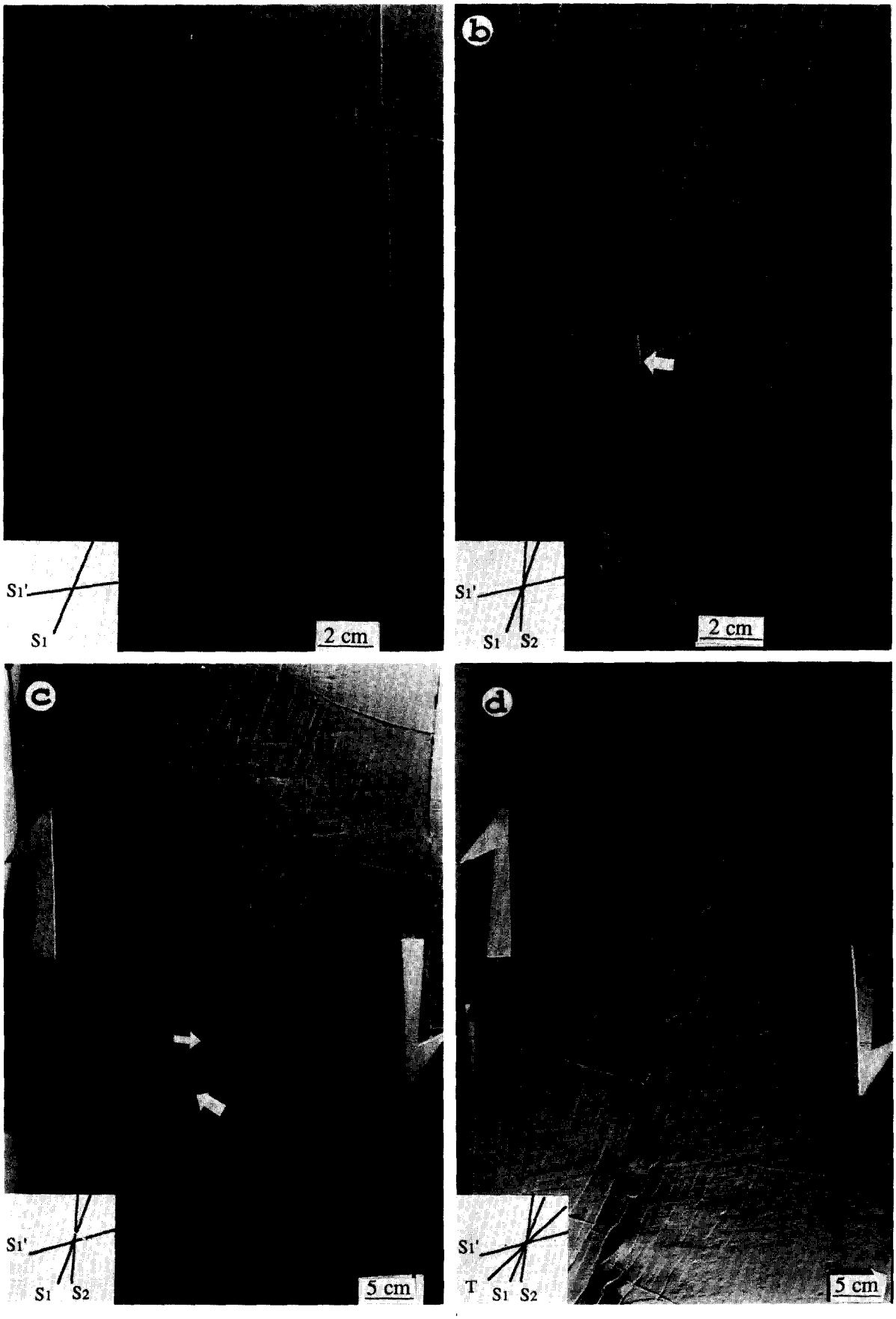

Fig. 3. Faults developed in a gouge layer under simple shear. At stage (a) the layer dilates. Faults nucleate as conjugate protofaults. Some faults also nucleate on visible pores. Note the long length and high density of the protofaults. At stage (b) primary shear sets S_1 and S_1' develop from the protofaults and pores. Some abandoned protofaults are visible between the primary shear faults. At the stage (c), secondary shear S_2 (one pointed out by a thin arrow) emerges at a few locations. S_1 develops further by in-plane growth and out-of-plane coalescence. The final stage is shown in (d), where a through-going shear zone has been developed.

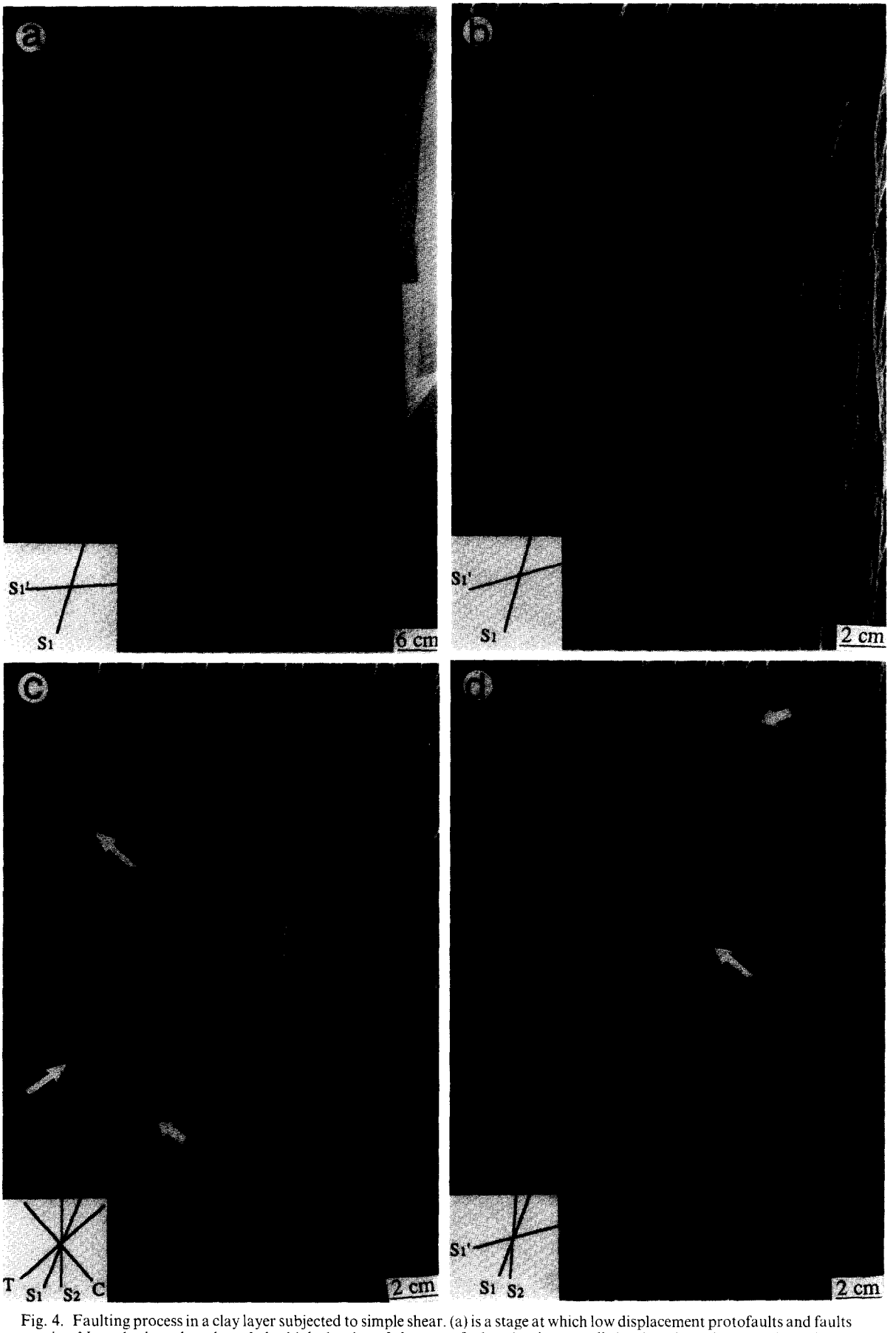

Fig. 4. Faulting process in a clay layer subjected to simple shear. (a) is a stage at which low displacement protofaults and faults coexist. Note the long length and the high density of the protofaults. (b) shows well developed S_1 shears and much less developed S_1' shears. (c) demonstrates the addition of secondary shear S_2 in the pattern which connects S_1 faults in left-step. Note C-lamella about perpendicular to S_1. Finally, in (d), a through-going shear zone is developed. The zone is most recognizable from the largest offset it carries. Disabled protofaults are visible between S_1 shears in (b), (c) and (d). Upwarps and rhombochasms are indicated by thin and fat arrows, respectively.

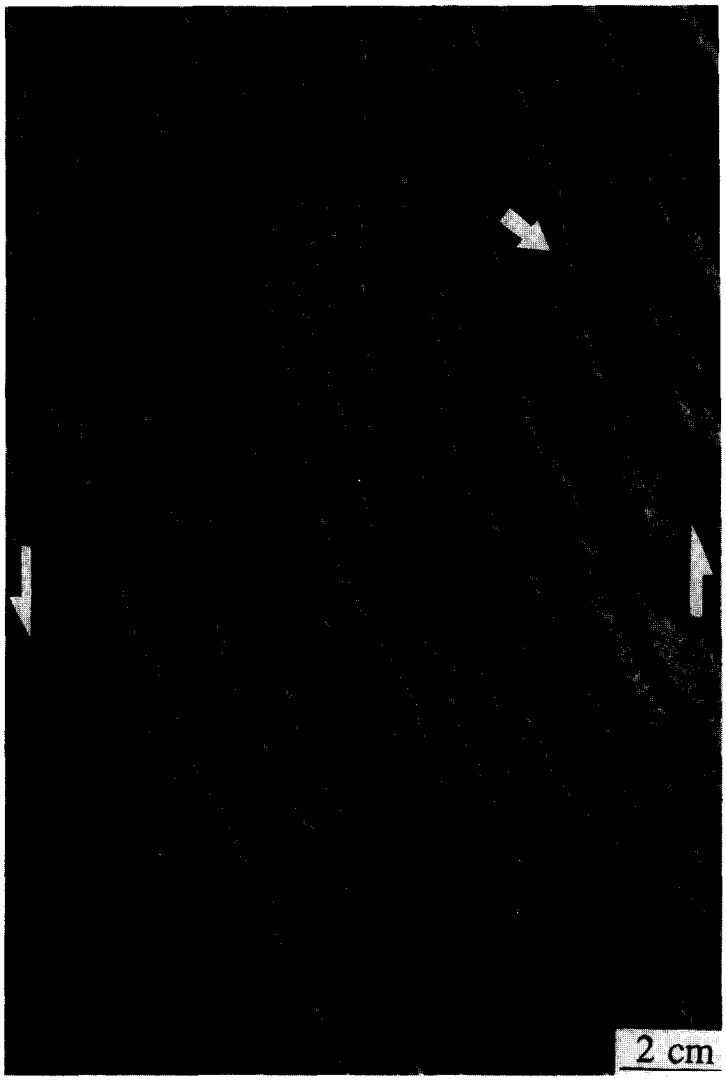

Fig. 5. Tips of simple faults and compound faults developed in a clay layer terminate as single protofaults, en echelon shear arrays, or horsetail fractures. The body of each fault contains many echelon micro fractures. Arrow points to a linear marker being offset by shear displacement along the structures. The marker was originally horizontal.

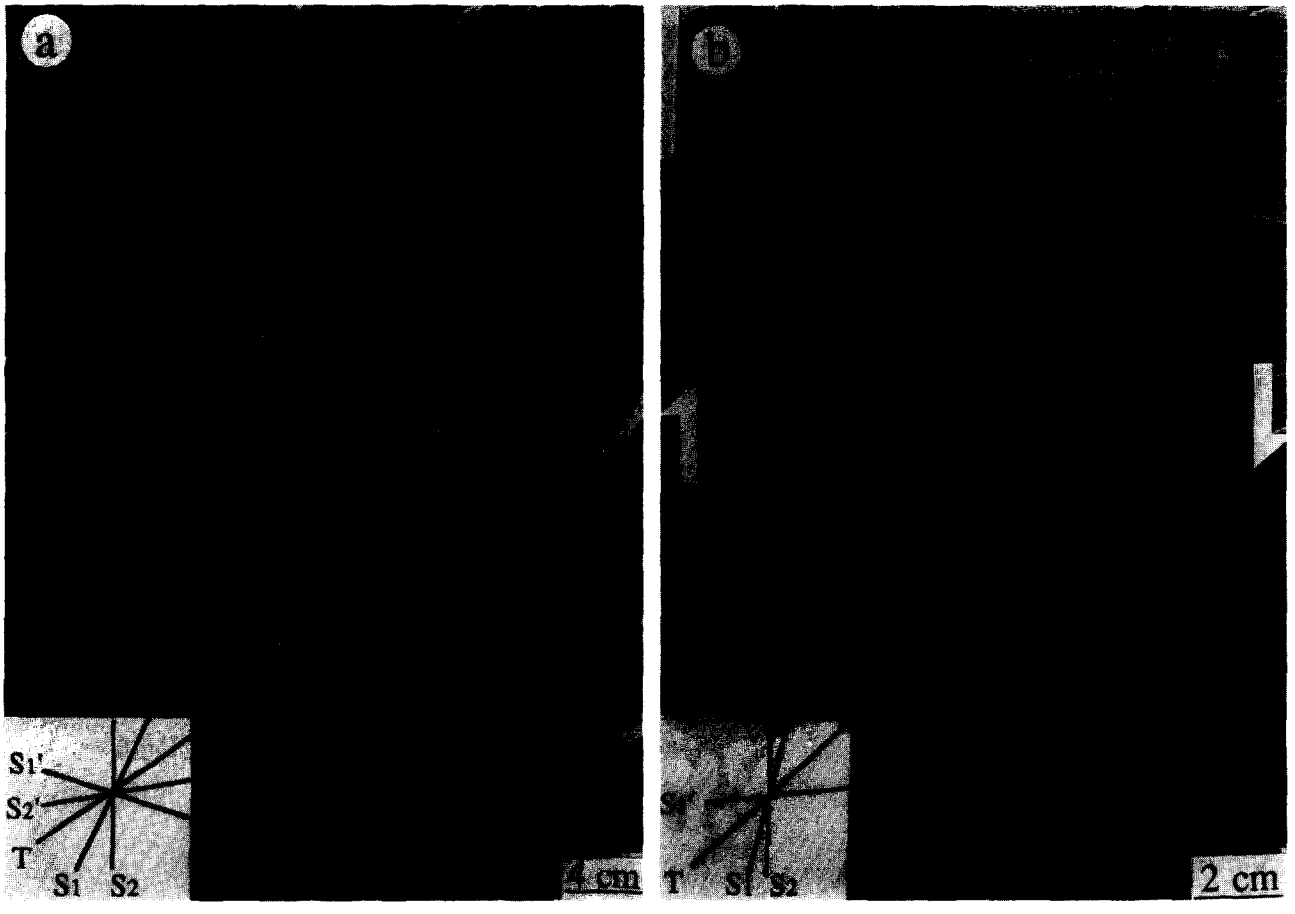

Fig. 6. (a) shows conjugate shear structures S_1 and S_1' cross over and intersect each other forming a fault grid. Fault domains in which one fault set is more developed than the other is also visible; (b) shows S_1 shears are coalesced by using S_1' and T structures forming releasing steps. Note the disabled protofractures between faults. Also note the formation of rhombochasms by fault offsetting along the steps.

Table 1. Faulting sequences under simple shear

stages	strain	structures (angles*)	coalescence	remarks
Gouge layer				
dilatation	~0.15	open pores, protofaults (21 ± 2/79 ± 2), micro shears	—	conjugate protofaults
primary shearing	~0.3	S_1 (22 ± 2) S_1' (80 ± 2)	S_1–S_1'	S_1–S_1' conjugate
secondary shearing	~0.4	S_2 (~1) rhombochasms	S_1–$S_1'S_1$–S_2	S_1 (21 ± 2) S_1' (83 ± 3)
TS** shearing	~0.5 [~0.4]	TS zone (~15), T (~50), rhombochasms	TS–S_1, TS–S_1', TS–S_2	S_1 (22 ± 2) S_1' (83 ± 4)
Clay layer				
dilatation	~0.15	open pores, protofaults (13 ± 2/82 ± 4), micro shears	—	conjugate protofaults & micro shears
primary shearing	~0.3	S_1 (14 ± 2) S_1' (84 ± 4)	S_1–S_1'	S_1–S_1' conjugate
secondary shearing	~0.36	S_2 (~0), C-lamella, rhombochasms, upwarps	S_1–S_1', S_1–S_2	S_1 (15 ± 2) S_1' (85 ± 4)
TS shearing	~0.39	TS zone (~7)	TS–S_1, TS–S_1', TS–S_2	S_1 (16 ± 3) S_1' (86 ± 4)

*The orientations of faults with respect to simple shear direction (clockwise in degrees).
**TS: through-going shear zone.

along the direction about 22° in the gouge layer and 13 ± 3° in the clay layer measured clockwise from the applied simple shear, and S_1' propagated along a direction about 80° in gouge and 84° in clay from the applied shear. The propagation tip of a simple fault was indistinct, gradually evolving into a low-displacement protofault and then disappearing. At the later stages, especially when the growth of simple faults stopped near the sample boundaries, more structures became visible at simple fault tips (Figs. 4 and 5). Small simple faults generally terminated as a single fracture, a protofault, or en echelon fracture arrays, while large simple faults terminated with horsetail or splay fractures. The horsetail fractures were mostly shear fractures similar to the major simple faults but some of them might have more tensile components because of slightly different orientations. Sometimes (see the longer arrow in Fig. 5) small fractures developed intensively in front of a simple fault tip, constituting a region similar to a 'breakdown zone' or 'process zone' (Friedman *et al.* 1972, Evans *et al.* 1977, Cox & Scholz 1988).

As numerous simple faults grew in length, they approached each other. At the same time, one or two sets of secondary conjugate shears S_2 and S_2', tensile structures T, and a set of compressional linear features we termed C-lamella developed in the space between the primary shears (Figs. 3c and 4c, S_2' is visible in Fig. 6a). Simple faults then began to interact.

Compound fault stage

Compound faults began to develop as simple faults started to interact and coalesce (Figs. 3c and 4c). The interaction and coalescence usually took place by taking advantage of existing structures. Occasionally a new bridge structure was created in a previously structure-free area. The earliest interaction was between the conjugate primary shear sets S_1 and S_1'. The two simple fault sets crossed over and offset each other, creating segmented fault traces (Figs. 3c and 6a). Later secondary conjugate shear sets S_2 and S_2', as well as tensile fault set T, were nucleated in the fault pattern (Fig. 3c and 4c). They were small faults developed only between the parallelogram frames formed by the simple faults and were terminated by the simple faults when they met them. But these faults were important bridge structures which linked larger faults during fault coalescence.

Fault coalescence was most common between simple faults within the S_1 set and was less frequent between the simple faults within the conjugate S_1' set. The S_1 shears were linked up through S_1, S_2, S_2' shears and tensile structures (T), forming a large compound fault (Figs. 3c and 4c). When coalescence occurred between two S_1 shears through an S_1' or T structure, a releasing step formed (Figs. 6b and 7a & b). When coalescence occurred between two S_1 shears through an S_2 shear, a 'restraining' step was formed (Figs. 4c and 7c). Such a restraining step was really a shear structure at the beginning but acquired a compressional component during displacement along the S_1 shears. No fault was observed to link with another fault through a compressional structure.

Fault coalescence was a major mechanism of fault growth following the initial in-plane propagation phase.

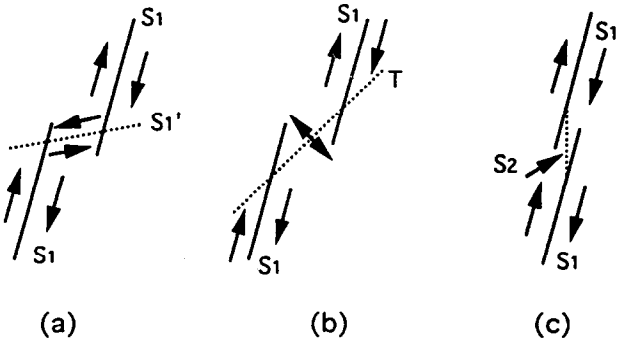

Fig. 7. Sketch showing coalescence of faults observed in the experiments. (a) and (b) show two S_1 shears are linked up by a S_1' shear and a T fracture, respectively, forming releasing steps. (c) shows two S_1 shears link up through a S_2 shear, creating a restraining step.

Coalescence not only made faults grow fast but also made the faulting process more chaotic. A short fault sometimes linked with a longer fault. But a longer fault sometimes grew very slowly because no coalescence occurred. In a fault pattern where numerous strike-slip faults competed to grow by propagation and coalescence, one fault emerged with the fastest growth rate. It spanned the region and became a through-going shear zone (Figs. 3d and 4d). This zone was again not parallel to the applied simple shear but formed at an angle (about 15° in gouge and 7° in clay) clockwise form the applied simple shear. Deformation became nonuniform upon the emergence of the through-going shear zone. Strain was predominantly accommodated by the through-going shear zones thereafter.

Fault patterns

Fault patterns are dynamic. Fault orientations illustrated in Fig. 8(a) and listed in Table 1 are the initial orientations of simple faults. These orientation changed during an experiment with progressive deformation. The orientations of simple faults and compound fault were different. For simple faults, those oriented at lower angle with respect to the applied simple shear (e.g. S_1 and S_2) rotated less than the structures oriented at higher angles (e.g. S_1' and S_2'). The maximum rotation recorded was for the experiment shown in Fig. 6(a) in which the S_1' set had rotated about 20° clockwise when it reached a strain of $\lambda = 1.5$. After this large rotation, most of the faults in the set stopped further development. For most other experiments, the rotation was only a few degrees (Table 1).

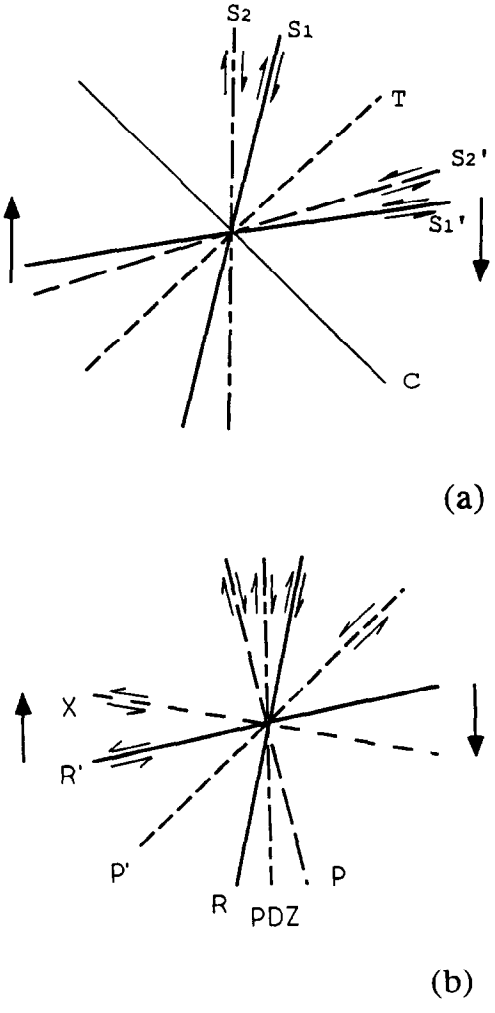

Fig. 8. (a) shows fault assemblages developed in our simple shear experiment. (b) shows the conventional Riedel model. PDZ: principal deformation zone.

Fault barriers and pull-apart basins

The compound faults had many bends (Figs. 3–6). The faults and fault segments inside a compound fault stepped both right- and left-laterally. Under the right-lateral shear, a right-step created a releasing step where fault walls were pulled apart forming rhombochasms, while a left-step in such an environment developed a restraining step where fault walls were pushed together (Fig. 4c & d). There were two types of releasing steps (Fig. 7). An $S_1 - S_1'$ type releasing step formed when two S_1 shears were linked up by a S_1' (or equivalently two S_1' shears were linked up through a S_1, Fig. 7a). A $S_1 - T$ type releasing step formed when two S_1 shears were linked up by a T fault (Fig. 7b). Under most circumstances, however, more restraining steps were formed than releasing steps in such a right-lateral shear condition. Two types of restraining steps were also observed (Fig. 9). A low-angle restraining step was formed when two S_1 shears coalesced through a S_2 shear (Figs. 3c and 4c, also Fig. 9a & b). A restraining step formed in this way was actually a shear-dominated structure, although upwarps (Fig. 4c & d) along such structures indicated that it had a compressional component. A high-angle restraining step was formed by conjugate shearing (e.g. in Fig. 6a S_1' shears were offset by S_1 shears forming such steps; also see Fig. 9c & d). Such a step was generally smaller in scale than the first type, but it constituted a major barrier to fault slip since it was almost perpendicular to the fault trace.

After shear displacement along a strike-slip fault with bends, the two fault walls became unmatched (Figs. 3d and 4d). The walls were in contact at the restraining steps (Fig. 9), and were pulled-apart along the releasing steps (Fig. 10a & b). The walls were also pulled-apart along regular shear segments (e.g. S_1) when shear displacement took place on a restraining step nearby (Figs. 3d, 4d and 10c). After several millimeters of shear displacement, the two walls of a compound strike-slip fault remained in contact at only a few restraining steps (Figs. 3d and 10d & e). These points were critical for further fault displacement and acted as fault barriers. Two types of barriers were recognizable corresponding to the two types of restraining steps (Fig. 9). A low-angle barrier had synthetic shear displacement (Fig. 9a & b). The contact area on such a barrier decreased with progressive shear displacement. Eventually the barrier was smoothed out, and new contacts occurred at other locations. On a high-

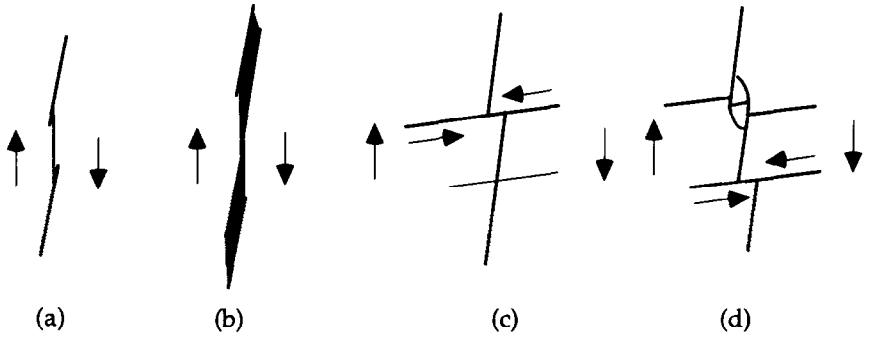

Fig. 9. Sketches showing two types of restraining steps observed in the experiments. (a) and (c) are the geometries before displacement and (b) and (d) show the geometry after displacement. In (d) an old high-angle restraining step is destroyed but a new one is created.

angle barrier shear displacement was almost perpendicular to the fault strike, and strike-parallel slip was not possible without breaking through the barrier (Fig. 9c & d). When the old barriers were broken, new barriers were created by conjugate shear displacement on another conjugate fault (Fig. 9d).

A pull-apart basin (rhombochasm) formed on a releasing step (type I) which was bounded either by four conjugate shear structures (*S*-type step, see Fig. 10a), or by two shears and two tensile structures (T-type releasing step, see Fig. 10b). A pull-apart basin formed near a restraining step (type II) was bounded on all sides by shear structures (Fig. 10c). The geometry of pull-apart basins changed with fault displacement. The type I pull-apart basins grew parallel to the fault strike, while the type II pull-apart basins grew oblique to fault strike. Generally type II basins were narrower but longer than type I. When confining pressure was added by tilting the loading board laterally, the type II basins were less developed. The two types of pull-apart basins always linked up forming larger compound basins along a fault trace as fault displacement increased further (Fig. 10d & e).

Comparison of fault development in the gouge and clay layers

The most significant difference between clay and gouge layers was the orientation of shear sets. In clay layers the angles between the applied shear and S_{1a} shear set was smaller but the angle between the applied shear and S_1' was larger (Table 1). The second difference was that both S_1' and T faults were more abundant, had longer fault lengths and larger displacements, (compare Figs. 3 and 4) in the gouge layer, but S_2 shears were more developed in clay layers. In the clay layer, a majority of S_1 shears were linked up by S_2 shears. The strike-slip faults formed in this way were closer to the applied shear direction than S_1 and had more shear component (Fig. 4d). In the gouge layer, S_1 shears were sometimes linked-up mostly by S_1' and T structures forming strike-slip faults. The strike-slip faults formed in such a way deviated farther from the applied shear than S_1 shear (Fig. 6b) and had a larger opening component. The third difference was that faults were denser in the clay layer where the average spacing between major faults was about 5 mm. In the gouge layer the average spacing was about 12 mm. Higher water content decreased fault spacing in both materials. Also notable was a set of dense but faint compressional surface lamellae in the clay which trended about 60° anticlockwise from the applied shear (represented by C in Fig. 4c).

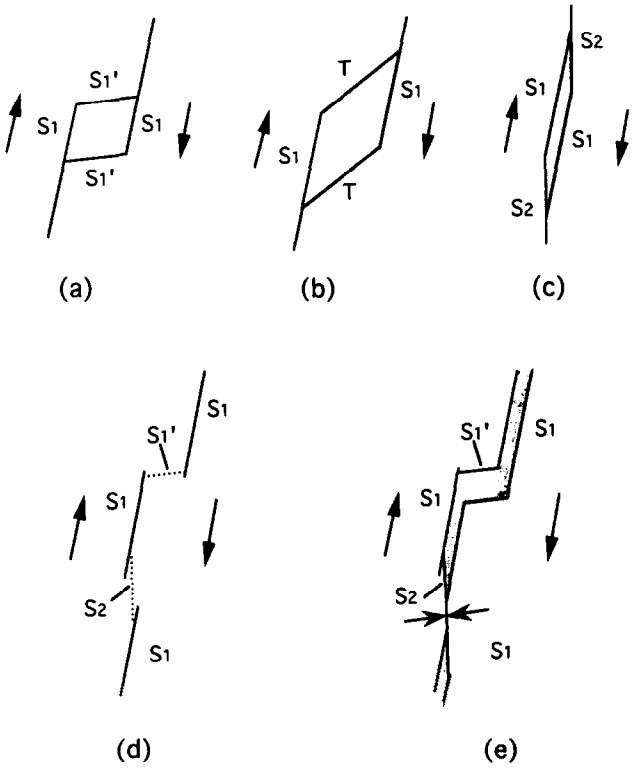

Fig. 10. Pull-apart basins are formed both by the displacement along releasing steps (a) and (b) and nearby restraining steps (c). In (a) and (c) the basins are bounded by shear structures; in (b) a basin is bounded by two shear structures and two T structures. Displacement along a strike-slip fault in (d) makes two fault walls contact only at one location while turning all the other parts into pull-apart basins, as shown in (e).

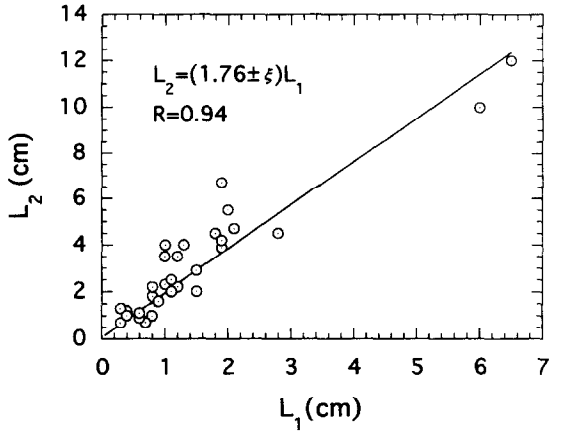

Fig. 11. Plot of initial length L_1 against final length L_2 for faults developed in a clay layer. The linear fitting of the data implies linear relationship between fault length and fault propagation rate. R is the correlation coefficient.

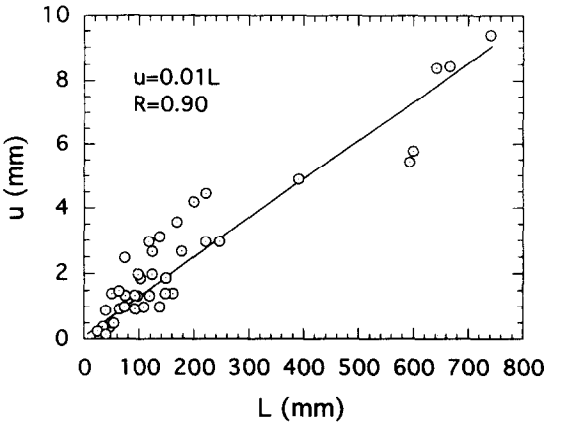

Fig. 12. Fault displacement u is plotted as a function of the fault length L. The linear fitting suggests that the maximum displacement of a fault is linearly related to its length. R is the correlation coefficient.

Scaling relationships between fault propagation rate and fault length

The relationship between fault propagation rates and fault lengths was studied by measuring the initial lengths of simple faults which didn't coalesce with other faults, L_1, on a photo taken at an early time in the fault evolution, and then measuring the lengths of the same simple faults, L_2, on a photo taken at a later time when shear strain had increased by ~ 0.2. When L_2 is plotted as a function of L_1 (Fig. 11), the data can be fit by a straight line $L_2 = (1.76 \pm \xi)L_1$, with a correlation coefficient R = 0.94. In other words, the length increment (ΔL) of a simple fault was linearly proportional to the original simple fault length (i.e., $\Delta L = CL_1$ where C is a constant related to the strain and hence $L_2 = (1 + C)L_1$ as observed). Since the propagation velocity $v = \Delta L/\Delta t$, where Δt was the time interval during which fault length was measured, and ΔL was a constant for all simple faults in the same pattern, v was also linearly proportional to fault length.

The linear relationship between fault propagation rate and fault length holds only for the simple faults not involving coalescence. At the later stages of our experiments when simple faults coalesced becoming compound faults, the fault length was no longer linearly related to the propagation rate.

Scaling relationships between fault displacement and fault length

We measured the length and maximum displacement of each independent fault on the deformed clay layer shown in Fig. 5(c). The maximum displacement was measured from the dislocated grid markers going through the middle portion of the faults. In Fig. 12 the fault displacement is plotted as a function of fault length. The linear fit with a correlation coefficient R = 0.9 yields a ratio of displacement/length of 0.01, which is in agreement with the ratio reported by Cowie & Scholz (1992). It also confirms the theoretical results that the maximum displacement on a fault is linearly correlated with the fault length (e.g. Pollard & Segall 1987).

DISCUSSION

Implications of protofaults

The development of protofaults may indicate that strike-slip faults can nucleate directly from defects (e.g. pores). The defects first produce dilatation which leads to strain hardening. They then may nucleate shear growth, and coalesce to form long protofaults. The high density of the protofaults in the moist clay and gouge indicates a large population of the active defects suggesting the pores themselves are responsible. The conjugate geometry of the protofaults and their orientations indicate that they are indeed shear structures.

Most of the protofaults are disabled after some of them grow into simple faults. This may suggest stress relaxation caused by shear displacement along the simple faults once they penetrate the layer. The spacing between simple faults seems to be controlled by layer thickness, water content and material. Initial observations indicate that a thicker layer with lower water content has larger spacing between simple faults.

It is still questionable if these structures can be observed in the Earth's crust. It is probable that protofaults cannot develop in near-surface prefaulted rocks, but they might develop in the rocks at depth as well as in soft sedimentary layers in basins. Rocks at depth are subject to large confining pressure and are less brittle. These conditions favor the development of shear structure. Some weak surfaces which evolve into straight, equally-spaced joints upon uplift may be related to protofaults formed earlier at depth. Some early foliation in metamorphic rocks may also share similarities with protofaults. Loose sediments in a sedimentary basin are the closest analogue to the granular materials used in the shear experiments. However small-scale protofaults can be easily erased or disturbed by topographic relief.

Mechanisms of in-plane propagation

In-plane propagation of shear cracks has been reported by Petit & Barquins (1988), Reches (1988), and Reches & Lockner (1994). However, the mechanism for in-plane propagation in their studies is in-plane damage of a series of tensile cracks. Such tensile crack arrays were not observed in our experiments. Rather we observed micro shear arrays (Fig. 5). The shear character was identified because the micro shears were almost parallel to the macro shear in which they existed, and they had different orientations in different fault sets. Such en echelon micro shear arrays were not observed at the early stage of fault development, but only when faults had acquired large displacement. Because of this observation, and because the newly nucleated faults emerged as thin and continuous protofaults oriented in conjugate shear directions, we conclude that in-plane shear propagation can take place independent of tensile fracturing. However this only occurs under certain conditions which we now elaborate.

Melin (1986) has proven theoretically that when confining pressure is high and internal crack pressure is low, a crack can propagate in-plane. Such a condition exists when a fault is a closed system: no material exchange occurs between a fault opening and its outside environment. In this case, a pressure drop within a crack due to crack opening will be maintained, and further opening displacement on the crack is suppressed by confining pressure when the internal pressure has dropped to a critical level. The pores within the moist clay and gouge are closed systems. They are isolated and sealed by both surrounding grains and surface tension in the water film between the grains (Fig. 13a). At the beginning, pore pressure P_p and confining pressure P_c were balanced. During a sample dilation, pressure within each pore dropped, creating a situation where confining pressure was larger than pore pressure ($P_c > P_p$). The dilation was eventually stopped when pore pressure had dropped so low that confining pressure and capillary pressure were able to suppress the dilation force (Fig. 13b). Further dilation by developing tensile faults in such an environment was not possible unless the pores were no longer sealed. On the other hand, because shear displacement did not cause as much expansion in the pore volume and therefore little pressure drop was involved, shear structures developed by coalescence of the low-pressure pores and subsequent grain boundary sliding (Fig. 13c). A similar process might occur in the crust where the combination of groundwater and lithostatic pressure suppress tensile extension except at very shallow levels (above the water table) where faults are not sealed and therefore they can propagate as tensile crack.

Angles of strike-slip faults

The major strike-slip faults do not develop parallel to the applied shear direction, and the deviation angle of a strike-slip fault from applied shear is larger in gouge than in clay. By analogy with the results of rock mechanics

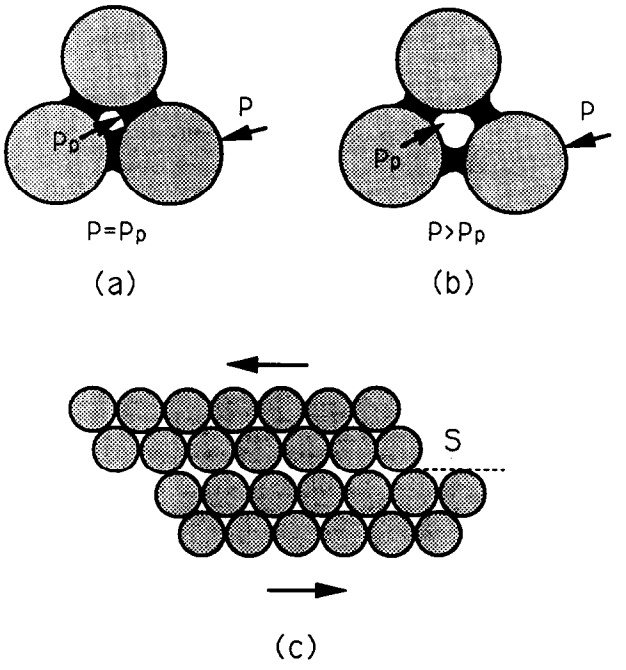

Fig. 13. Suggested mechanism for the nucleation and propagation of shear structures in moist granular materials. (a) shows a pore is sealed by stagnated water, (b) shows the dilation of the pore is stopped by pore pressure drop, and (c) shows how several such pores might coalesce permitting grain boundary sliding, nucleating a shear fault.

experiments under axial loading (Jaeger & Cook 1976), we propose that the departure was caused by the internal friction of clay and gouge layers. The different angles observed in clay and fault gouge were related to the different friction properties of these materials, which may be related to different grain sizes and minerals. The layers with coarse grains (gouge) had a larger deviation angle.

The quantitative departure from the applied shear direction, α, can be estimated from the coefficient of friction, μ. According to Jaeger & Cook (1976), the friction angle, ϕ, of a material equals

$$\phi = \tan^{-1}\mu. \tag{3}$$

A shear plane would occur in the direction θ, from the principal stress σ_1:

$$\theta = \frac{\pi}{4} - \frac{\phi}{2} \tag{4}$$

where the second term on the right hand side represents the departure angle from applied shear, i.e.

$$\alpha = \frac{1}{2}\phi = \frac{1}{2}\tan^{-1}\mu. \tag{5}$$

For moderately rough surfaces of typical rocks, the value of μ is between 0.51 and 0.75 (Jaeger & Cook 1976). This gives α = 12°–18°. The friction coefficient of clay and gouge layers with water content at 39% by weight is not known. Our experiments indicate, however, that they are almost the same as that of rocks because α is 14°–22°. A direct-shear experiment conducted by Sims (1993) for a moist clay with 50% H_2O by weight indicates a value of ϕ = 28°, corresponding to α = 14° (i.e. shear failure plane is 31° from σ_1). It seems that internal friction

of a granular material is not so sensitive to water content but is sensitive to grain size (and possibly shape).

Comparison with Riedel shear experiments

The Riedel shear experiment (Cloos 1928, Riedel 1929) is the earliest and most traditional method to study strike-slip faults in the laboratory. It is still widely used in recent studies (Tchalenko 1970, Wilcox *et al.* 1973, Naylor *et al.* 1986, Richard & Krantz 1991, Richard *et al.* 1991, Smith & Durney 1992). The core components of the experiment are the two parallel blocks that can slide parallel to each other. Structures are developed in model material above the blocks as they slide. Riedel experiments have produced the structures shown in Fig. 8(b). The first structures to form are a conjugate pair of synthetic and antithetic shear structures known as Riedel shear and conjugate Riedel shear (R and R′ in Fig. 8(b)). These are followed by secondary synthetic shear structures denoted by P. Another secondary antithetic structure, X, which is conjugate to P, was proposed by Bartlett *et al.* (1981). However, Naylor *et al.* (1986) argued that the X structures may have been rotated primary antithetic faults, R′. The real conjugate structures to P should be P′, where the bisector of the secondary conjugates is parallel to the primary synthetic fault and that the change from primary to secondary fault is a result of stress reorientation. Neither the X nor P′ structures have been conclusively documented.

We found that our primary shear S_1 and the conjugate primary shear S_1' correspond to the Riedel shear R and the conjugate Riedel shear R′, respectively. However, we have not observed any through-going shear zone (similar to PDZ in Fig. 8b) parallel to the applied shear direction. We also have not observed X, P and P′ structures in our experiments. One set of shear structures trended in the X direction at a later stage of fault evolution (Fig. 6a). However, it was identified as a set of rotated S_1' but not a new shear set. By comparison, we found that our secondary shear structure S_2 lay in a direction corresponding to that of PDZ in Riedel experiment, and our secondary conjugate shear S_2' had an orientation very close to that of R′ (Fig. 8a). They are both in the quadrant occupied by R and R′. No strike-slip fault was observed within the quadrant where P is supposed to develop in Fig. 8(b) except S_1' which sometimes rotated a little toward that direction. At times normal faults developed in our experiments in a direction close to the secondary conjugate shear P′ in Riedel shear experiment.

All the trends of the structures in our experiments evolved with added shear strain. For example, as S_1' rotated away from its initial position and could no longer accommodate strain efficiently, S_2' occurred close to the original S_1' direction (Fig. 6a). We observed that as S_1' rotated to the position of X in Fig. 8b, T structures were in the P′ position. We suspect thus that X and P′ in Riedel experiments are not new, but rotated S_1' and T in our experiments, respectively.

We consider the differences between our experimental results and Riedel model are due to the different boundary conditions. In Riedel shear a pre-existing 'fault' (the block boundaries) is active underneath the clay layer. All the deformation in the clay layer is caused by the movement on the pre-existing 'fault'. Therefore the structures developed in the top layer are secondary with respect to this fault. The through-going shear zone is not independently developed. Thus the Riedel experiment may only be suitable for studying surface ruptures caused by blind faults which are covered by a sedimentary layer. Our experiments did not have a pre-existing fault as a boundary condition. Fault nucleation, growth and stepping were well exhibited. Therefore our model may be more appropriate for studying the nucleation and evolution of strike-slip faults in broad shear zones.

Comparison with previous distributed shear experiments

Previous distributed shear experiments generated distributed synthetic shear, R, antithetic shear, R′, and P structures (corresponding to our S_1, S_1' and S_2, respectively). The faults were initially straight, then became non-linear. Most of the faults were regularly spaced. Different fault patterns were generated by the different investigators. Cloos (1955) generated fault patterns in which two sets of primary shear sets were almost equally developed; Hoeppener *et al.* (1969) generated fault patterns dominated by antithetic shear set; and Freund (1974) and Schreurs (1992, 1994) generated fault patterns dominated by synthetic shear set. Schreurs (1992) suggests that differences in the initial dimensions of the samples might be responsible for the different fault patterns. If a sample is initially rectangular (as in Freund 1974 and Schreurs 1992, 1994), synthetic faults will dominate; if a sample is initially circular or square (as the ones used by Hoeppener *et al.* 1969), antithetic faults will dominate.

Our experiments confirmed S_1 and S_1' (corresponding to R and R′ in previous experiments) as dominant structures in a distributed fault pattern. We also noticed faults change from straight to non-linear as the fault pattern evolved. We attribute this bending to fault coalescence and rotation. We further noticed a fundamental difference between simple faults and compound faults. A simple fault has a definite orientation (although it rotates with strain) while a compound fault does not because a compound fault contains coalesced segments of simple faults of different types. A compound fault is the closest analogue to a natural strike-slip fault. We observed the development of fault bends and pull-apart basins.

All the fault patterns generated in our experiments were dominated by synthetic faults although we used both square and rectangular samples in our experiments. Therefore initial sample dimension might not be the essential factor which controls fault patterns. A similar observation can be made in the Cloos (1955) experiments in which approximately circular clay cakes were used. Synthetic and antithetic faults were almost equally developed in the final fault patterns.

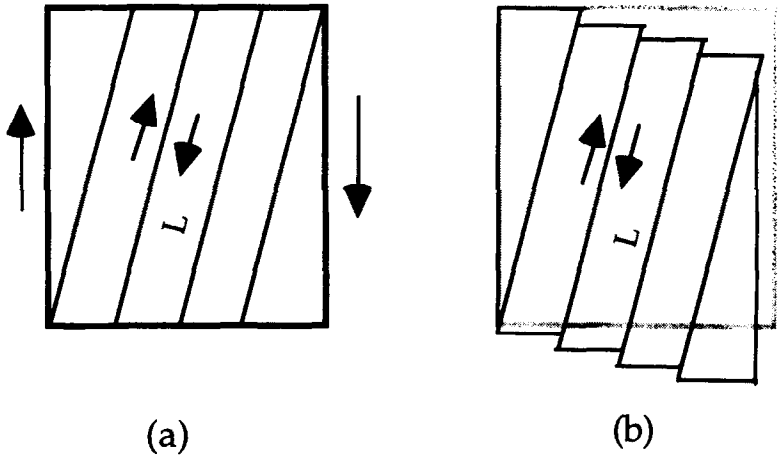

Fig. 14. Diagrams showing geometrical change during the development of a synthetic fault-dominated pattern. Slip on synthetic faults requires lateral shortening. Slice length, L, is assumed constant.

We suggest an alternative explanation for the observation of different fault patterns. From a purely geometrical point of view, slip along synthetic faults will lead to lateral shortening of a sample (Fig. 14a & b), and slip along a set of antithetic faults will first lead to initial lateral expansion of the sample (Fig. 15a & b) and then, after the antithetic faults rotate passing the perpendicular direction to the applied shear, the sample begins to shorten (Fig. 15b & c). From this point of view it seems that if a sample is not allowed to shorten in the lateral direction during a shear deformation (as in the experiment conducted by Hoeppener *et al.* 1969), antithetic faults will predominantly develop, and if a sample is allowed to shorten laterally (as in the experiments performed by Cloos 1955, and in this paper), synthetic faults will preferably develop. An example was provided by Gapais *et al.* (1991) who used square-shaped samples in all their experiments. When the sample was not allowed to shorten in the lateral direction, antithetic faults prevailed in the fault patterns; when the lateral was shortened laterally, synthetic faults became dominant. Exceptions to this explanation are the experiments performed by Freund (1974) and Schreurs (1992, 1994) who used stacks of sliding bars to apply simple shear stress to the overlying samples. Although lateral shortening was not allowed in such experimental setup, synthetic faults dominated their fault patterns. Our explanation is that the bars in the stacks can only slide parallel to each other while they resist lateral movement of the sample above. Therefore synthetic faults should be the most developed structures.

Similarities between the experiment and crustal conditions

In regions of intense deformation, the upper brittle layer of the Earth's crust may be thought of as granular (Scott *et al.* 1993). Faults, fractures, joints, beds, foliations, and cleavages cut the brittle crust into blocks over a wide range of scales. Similar to moist clay and gouge, the grains are saturated or partially saturated with water when they are below the water table. Unlike moist clay and gouge, these grains are larger and more irregular. However at depth, the gashes between the grains might not be much larger than the pore size in the

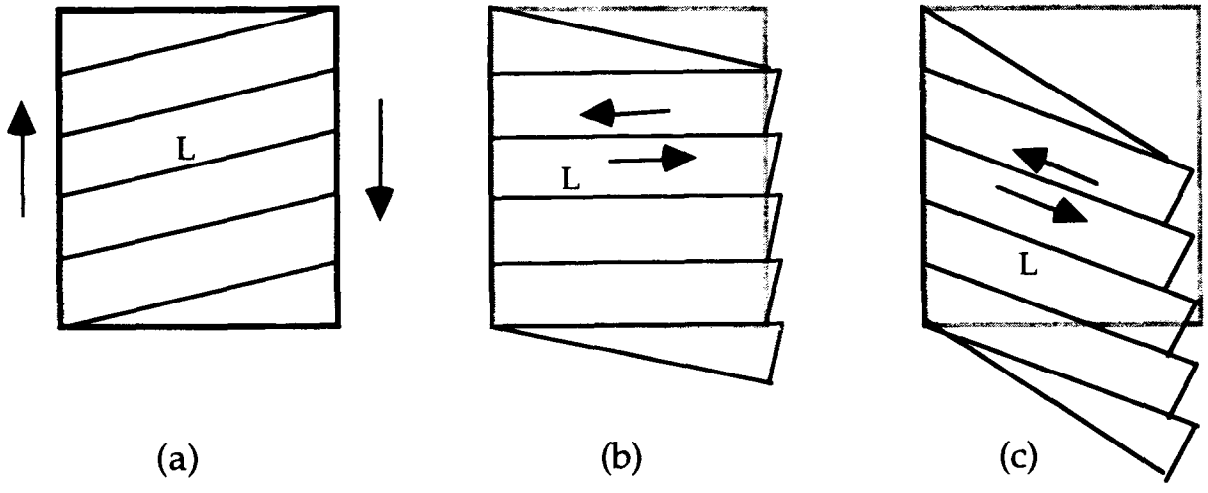

Fig. 15. Diagrams showing geometrical change during the development of an antithetic fault dominated pattern. Slip on antithetic faults leads to lateral expansion before the antithetic faults rotate to lie perpendicular to the applied shear. After this point, the sample begins to shorten laterally. Slice length, L, is assumed constant.

clay and gouge samples due to high confining pressure. Therefore our experiments and the brittle layer of the crust may have similar material properties.

The lower ductile crust is more cohesive due to high temperature and confining pressure. An & Sammis (1994) estimated, by considering capillary pressure in a granular material, that when grain size becomes smaller, the granular material become more cohesive. The effect of decreasing particle size is therefore similar to increasing confining pressure: make a granular material more cohesive. The confining pressure in the crust is thus simulated. Additionally, a strike-slip fault in the crust is really an anti-plane shear. A discontinuous fault plane gradually terminates in the lower ductile crust. The upper brittle crust and the lower ductile crust are coupled. The movement along the fault in the upper brittle layer might be dragged by the lower ductile layer. This coupling effect is simulated by the basal friction in our experiment which always resists fault movement. These many similarities suggest that the experiment may offer a reasonable analog for the development of faults.

CONCLUSIONS

The shear experiments with moist clay and fault gouge layers demonstrated that:

(1) Protofaults developed in conjugate sets upon nucleation. The competing growth of the protofaults changed some of them into simple faults while disabling most of the others. Some simple faults nucleated directly from pores.

(2) Once nucleated, simple faults propagated in plane. The tip of a simple fault gradually became complicated by echelon or horsetail fractures as it grew longer but a majority of the fractures were shear fractures.

(3) Simple strike-slip faults coalesced forming compound strike-slip faults. Coalescence occurred most often by taking advantages of existing minor simple faults in the same fault pattern. Both releasing- and restraining-steps were developed during coalescence. A low-angle restraining step was actually a shear dominated structure.

(4) A typical fault pattern consisted of a fault grid made of several generations of conjugate simple faults, compound faults, and tensile structures. The primary generation of conjugate strike-slip faults established the framework within which later generations were added. A through-going shear zone emerged from the most developed synthetic fault set.

(5) Major strike-slip faults did not develop parallel to the direction of applied simple shear stress. A through-going strike-slip fault had a deviation angle equal to $\sim 8^\circ$ in clay and $\sim 16^\circ$ in gouge. The deviation probably resulted from the internal friction of the materials and increased with greater grain size.

(6) Dynamic displacement along a strike-slip fault caused mismatch of the two fault walls which left a few contact points as resistant barriers and turned most of the other parts into pull-apart basins. Both releasing and low-angle restraining steps led to the formation of pull-apart basins.

(7) The propagation rate of simple faults and displacement along faults are both linear functions of fault length.

(8) Differences were observed in fault development between the clay and gouge layers: in the clay layer, major strike-slip faults were closer to the applied shear direction, antithetic primary shears were fewer and weaker, but synthetic secondary shears were more numerous and stronger than those in the gouge layer. Tensile structures were more often developed in the gouge layer. The clay had finer grain size and was more coherent than the gouge.

Comparison between the experimental and the crustal conditions suggests that the experimental observations can be relevant to the study of crustal shear zones.

Acknowledgements—We thank J. P. Evans, D. McConnell, P. Umhoefer, G. Schreurs, and an anonymous reviewer for their critical comments which helped improve the quality of the paper. We also thank G. A. Davis and G. Schreurs for bringing relevant literature on simple shear to our attention. This study was supported by United States Geological Survey contract 1434-94-G-2438.

REFERENCES

An, L.-J. & He, Y. 1987. Estimate of differential flow stress and strain rate in Honghe (Red River) fault zone, *Seism. & Geol.* **9**, 53–59 (in Chinese with English abstract).

An, L.-J. & Sammis, C. G. 1994. Particle size distribution in cataclastic fault materials from Southern California: a 3-D study. *Pure Appl. Geophys* **143**, 203–228.

Aydin, A. & Schultz, R. A. 1990. Effects of mechanical interaction on the development of strike-slip faults with echelon patterns. *J. Struct. Geol.* **12**, 123–129.

Bartlett, W. L., Friedman, M. & Logan, J. M. 1981. Experimental folding and faulting of rocks under confining pressure, Part IX. Wrench faults in limestone layers. *Tectonophysics* **79**, 255–277.

Brace, W. F. & Bombalakis, E. G. 1963. A note on brittle crack growth in compression. *J. geophys. Res.* **68**, 3706–3713.

Carter, N. L. & Tsenn, M. C. 1987. Flow properties of continental lithosphere. *Tectonophysics* **136**, 27–63.

Chang, R. 1982. On crack–crack interaction and coalescence in fatigue. *Eng. Fract. Mech.* **16**, 683–693.

Chen, Y. Z. 1984. General case of multiple crack problems in an infinite plate. *Eng. Fract. Mech.* **20**, 591–597.

Cloos, H. 1928. Experiment zur inneren Tektonic. *Centralbl. f. Mineral. u. Pal.* **1928B**, 609–621.

Cloos, E. 1955. Experimental analysis of fracture patterns. *Bull. geol. Soc. Am.* **66**, 241–256.

Cox, S. J. D. & Scholz, C. H. 1988. On the formation and growth of faults: An experimental study. *J. Struct. Geol.* **10**, 413–430.

Cowie, P. A. & Scholz, C. H. 1992. Displacement–length scaling relationship for faults: data synthesis and discussion. *J. Struct. Geol.* **14**, 1149–1156.

Crowell, J. C. 1974. Origin of late Cenozoic basins in southern California. In: *Tectonics and Sedimentation* (edited by Dickinson, W. R.), *Soc. Econ. Paleont. Mineral. Spec. Paper* **22**, 190–201.

Deng, Q., Wu, D., Zhang, P. & Chen, S. 1986. Structure and deformational character of strike-slip fault zones. *Pure Appl. Geophys.* **124**, 204–223.

Du, Y. & Aydin, A. 1991. Interaction of multiple cracks and formation of echelon crack arrays. *Int. J. Num. Anal. Mthds. Geomech.* **15**, 205–218.

Du, Y. & Aydin, A. 1993. The maximum distortional strain energy density criterion for shear fracture propagation with applications to the growth paths of en echelon faults. *Geophys. Res. Lett.* **20**, 1091–1094.

Evans, A. G., Heuer, A. H. & Porter, D. L. 1977. The fracture toughness of ceramics, *Proc. 4th Int. Conf. on Fracture*, Waterloo, Canada, 529–556.

Friedman, M., Handin, J. & Alani, G. 1972. Fracture-surface energy of rocks. *Int. J. Rock Mech. Min. Sci.* **9**, 757–766.

Freund, R. 1974. Kinematics of transform and transcurrent faults. *Tectonophysics* **21**, 93–134.

Gallagher, J. J., Jr. 1981. Tectonics of China: continental scale cataclastic flow. In: *Mechanical Behavior of Crustal Rocks* (edited by Carter, N. L., Friedman, M., Logan, J. M. & Stearns, D. W.). *Am. Geophys. Union, Geophysical Monograph* **24**, 259–274.

Gapais, D., Fiquet, G. & Cobbold, P. R. 1991. Slip system domains, 3. New insights in fault kinematics from plane-strain sandbox experiments. *Tectonophysics* **188**, 143–157.

Hildebrand-Mittelfeldt, N. 1979. Deformation near a fault termination, Part I. A fault in a clay experiment. *Tectonophysics* **57**, 131–150.

Hoeppener, R., Kalthoff, E. & Schrader, P. 1969. Zur physikalischen Tektonik: Bruchbildung bei verschiedenen affinen Deformationen im Experiment. *Geologische Rundschau* **59**, 179–193.

Horii, H. & Nemat-Nasser, S. 1985. A simple technique of stress analysis in elastic solids with many cracks. *Int. J. Fract.* **28**, 731–745.

Ito, H. 1983. Creep of rock based on long-term experiments. *5th Int. Congr. on Rock Mechanics*. Melbourne, Preprints, Section A, A117–A120.

Jaeger, J. C. & Cook, J. G. W. 1976. *Fundamentals of Rock Mechanics*, 2nd edn. Methuen, London.

Kachanov, L. M. 1987. Elastic solids with many cracks: a simple methods of analysis. *Int. J. Solids Struct.* **23**, 23–43.

Lajtai, E. Z. 1971. Experimental evaluation of the Griffith theory of brittle failure. *Tectonophysics* **11**, 129–156.

Lin, P. & Logan, J. M. 1991. The interaction of two closely spaced cracks: a rock model study. *J. geophys. Res.* **96**, 21,667–21,675.

Martel, S. J. 1990. Formation of compound strike-slip fault zones at Mount Abbot quadrangle, California. *J. Struct. Geol.* **12**, 869–882.

Melin, S. 1986. When does a crack grow under mode II conditions? *Int. J. Fract.* **30**, 103–114.

Mitchell, J. K. 1993. *Fundamentals of Soil Behavior*, 2nd edn. John Wiley & Sons, Inc., New York.

Naylor, M. A., Mandl, G. & Sijpesteijn, C. J. K. 1986. Fault geometries in basement-induced wrench faulting under different initial stress states. *J. Struct. Geol.* **8**, 737–752.

Peng, S. & Johnson, A. M. 1972. Crack growth and faulting in cylindrical specimens of Chelmsford granite. *Int. J. Rock Mech. Min. Sci.* **9**, 37–86.

Petit, J. P. & Barquins, M. 1988. Can natural faults propagate under mode II conditions? *Tectonics* **7**, 1243–1256.

Pfiffner, O. A. & Ramsay, J. G. 1982. Constrains on geological strain rates: arguments from finite strain states of naturally deformed rocks. *J. geophys. Res.* **87**, 311–321.

Pollard, D. D. & Segall, P. 1987. Theoretical displacements and stresses near fractures in rocks, with applications to faults, veins, dikes and solution surfaces. In: *Fracture Mechanics of Rocks* (edited by Atkinson, B. K.). Academic Press, London, 277–347.

Ramberg, H. 1981. *Gravity, Deformation and the Earth's Crust*, 2nd edn. Academic Press, London.

Reches, Z. 1988. Evolution of fault patterns in clay experiments. *Tectonophysics* **145**, 141–156.

Reches, Z. & Lockner, D. A. 1994. Nucleation and growth of faults in brittle rocks. *J. geophys. Res.* **99**, 18,159–18,173.

Richard, P. & Krantz, R. W. 1991. Experiments on fault reactivation in strike-slip mode. *Tectonophysics* **188**, 117–131.

Richard, P., Mocquet, B. & Cobbold, P. R. 1991. Experiments on simultaneous faulting and folding above a basement wrench fault. *Tectonophysics* **188**, 133–134.

Riedel, W. 1929. Zur Mechanik geologischer Brucherscheinungen. *Zentralbl. Mineral., Abt.*, 354–368.

Sammis, C. G. & Ashby, M. F. 1986. The failure of brittle porous solids under compressive stress states. *Acta metall.* **34**, 511–526.

Sammis, C. G., King, G. C. P. & Biegel, R. C. 1987. The kinematics of gouge deformation. *Pure Appl. Geophys.* **125**, 777–812.

Schreurs, G. 1992. Analogue modeling using X-ray computed tomography analysis: experiments on distributed strike-slip shear deformation. Institut Fracais du Pétrole Publ. Nr. 39893, Rueil Malmaison, France, 233.

Schreurs, G. 1994. Experiments on strike-slip faulting and block rotation. *Geology* **22**, 567–570.

Segall, P. & Pollard, D. D. 1980. Mechanics of discontinuous faults. *J. geophys. Res.* **85**, 4337–4350.

Segall, P. & Pollard, D. D. 1983. Nucleation and growth of strike slip faults in granite. *J. geophys. Res.* **88**, 555–568.

Scott, D. R., Forrest, M. R. & Sammis, C. G. 1993. Granular tectonics of southern California. *EOS, Trans. Am. geophys. Un.* **74**, 429.

Shen, B., Stephansson, O., Einstein, H. H. & Ghahreman, B. 1995. Coalescence of fractures under shear stresses in experiments. *J. geophys. Res.* **100**, 5975–5990.

Sibson, R. H. 1985. Stopping of earthquake ruptures at dilational fault jogs. *Nature* **316**, 248–251.

Sims, D. 1993. The rheology of clay: a modeling material for geologic structures. *EOS, Trans. Am. geophys. Un.* **74**, 569.

Smith, J. V. & Durney, D. W. 1992. Experimental formation of brittle structural assemblages in oblique divergence. *Tectonophysics* **216**, 235–253.

Sylvester, A. G. 1988. Strike-slip faults. *Bull. geol. Soc. Am.* **100**, 1666–1703.

Tchalenko, J. S. 1970. Similarities between shear zones of different magnitudes. *Bull. geol. Soc. Am.* **81**, 1625–1640.

Turcotte, D. L. 1991. Earthquake prediction. *A. Rev. Earth Planet. Sci.* **19**, 263–281.

Wang, J. S. Y. 1991. Flow and transport in fractured rocks. *Rev. Geophys.* **29**, 254–262.

Wesnousky, S. G. 1989. Seismological and structural evolution of strike-slip faults. *Nature* **335**, 340–342.

Wilcox, R. E., Harding, T. P. & Seely, D. R. 1973. Basic wrench tectonics. *Bull. Am. Ass. Petrol. Geol.* **57**, 74–96.

Withjack, M. O. & Jamison, W. R. 1986. Deformation produced by oblique rifting. *Tectonophysics* **126**, 99–124.

Yang, M. & Toksoz, M. N. 1981. Time-dependent deformation and stress relaxation after strike slip earthquakes. *J. geophys. Res.* **86**, 2889–2901.